UC Irvine

UC Irvine Electronic Theses and Dissertations

Title

Third Order Exceptional Point of Degeneracy in Coupled Resonators at Radio Frequencies

Permalink

https://escholarship.org/uc/item/8458v5bm

Author

Alshetaiwi, Muhannad

Publication Date

2018

Peer reviewed|Thesis/dissertation

eScholarship.org Powered by the California Digital Library
University of California

UNIVERSITY OF CALIFORNIA,
IRVINE

Third Order Exceptional Point of Degeneracy in Coupled Resonators at Radio Frequencies

THESIS

submitted in partial satisfaction of the requirements
for the degree of

MASTER OF SCIENCE

in Electrical Engineering and Computer Science

by

Muhannad Romaih S Alshetaiwi

Thesis Committee:
Professor Filippo Capolino, Chair
Professor Michael Green
Associate Professor Ozdal Boyraz

2018

© 2018 Muhannad Romaih S Alshetaiwi

DEDICATION

To

my parents

TABLE OF CONTENTS

LIST OF FIGURES

ACKNOWLEDGMENTS

I would like to express my deepest gratitude to my major advisor, Professor Filippo Capolino, who has the qualities of a great mentor and a prodigious scientist. He has given me this unique opportunity to work under his inspiration and dedication that helped me maintain my attention and raise my abilities. Without his guidance and persistent help this thesis would not have been possible. In addition, I would like to thank my committee members, Professor Michael Green and Professor Ozdal Boyraz for their valuable inputs throughout my research.

My special thanks go to my parents, Romaih and Loulwah, who has always stood by me and taught me at every step through my life to shape into the person that I am today. Many thanks also go to my uncle and roommate Hamad Alshetaiwi and my brothers, Mansour, Saleh, and Safwan, and my sisters, Reem, Reham, and Amera for their support and motivation.

I greatly thank my colleagues who were involved in this research, Hamidreza Kazemi, Mohammed Othman, and Mohamed Y. Nada and also my labmates Ahmed Almwtawah, Mehdi Veysi, Farshad Yazdi, Dmitry Oshmarin, Ahmed F. Abdelshafy, Tarek Mealy, and Puxi Zhou.

ABSTRACT OF THE THESIS

Third Order Exceptional Point of Degeneracy in Coupled Resonators at Radio Frequencies

By

Muhannad Romaih S Alshetaiwi

Master of Science in Electrical Engineering and Computer Science

University of California, Irvine, 2018

Professor Filippo Capolino, Chair

Operation mechanism of many novel sensors is based on the detection of splitting of resonant frequencies. Recently emerged topic known as exceptional points of degeneracy (EPD) paves the way to engineer structures where they exhibit highly sensitive frequency splitting phenomenon. An EPD is a special point in the system parameter space at which at least two eigenmodes coalesce in both their eigenvalues and eigenvectors. The unique properties of higher order EPD can provide means of enhancing the frequency shift as they would increase the effect of perturbation which should lead to higher sensitivity. In this dissertation, we propose a circuit comprised of three RLC coupled resonators with balanced loss and gain that exhibits a third order EPD and investigate the conditions for a third order EPD to occur in such circuit. We validate the existence of the EPD by examining the behavior of the system at that special point. We finally illustrate the time domain response of such system operating at regular frequency (not an EPD frequency) and also at a third order EPD frequency where we show the quadratic growth of the system eigenstates in time.

CHAPTER 1

INTRODUCTION

Sec. 1.1 Exceptional Points of Degeneracy (EPD):

Many sensing applications use the phenomenon of frequency splitting where this technique can be extremely enhanced exploiting systems with exceptional points of degeneracy (EPDs) [1]-[2]. The occurrence of the phenomenon is at the frequencies of degenerate resonance that is highly sensitive to small perturbations. Such is common where multiple system eigenmodes coalesce and there is variability in the shift that is detectable for the involved variables. Although in certain physics literature [3]–[7] such a condition is referred to as “EP” which may be indistinct to some other research communities, it is at this point that we add a “D” as “degeneracy” in the acronym to specify the kind of points we are referring to. The concept has a wide application in the current devices for sensing that include optical microcavities [2], [8], [9], sensors in the bending curvature [10] and the optical gyroscopes.

The point of splitting of the resonance degenerate frequencies varies with the parameters of the system and emerges when there is coalescence of two or more eigenmode in both eigenvectors and eigenvalues to generate the single eigenmode. In the past years, EPDs concept has attracted a great interest among the researchers [11]–[18]. EPDs occur only if the system matrix has a special degeneracy and are known to possess a condition of

eigenvectors of the system which is non-Hermitian. These have been evidenced in the non-Hermitian parity-time (PT-) symmetric systems that are coupled i.e. systems which have balanced loss and gain [12], [14], [17], [19].

PT-symmetry as it is related to the EPDs concept has received research that focuses on the eigenmodes evolution description in terms of space [1], [11], [20]. There is also the illustrated of the coupled resonators that use time to describe the evolution of the eigenmodes [13], [15], [16]. PT-symmetry theories have been employed in optics; resulting in remarkable properties been observed in coupled waveguides and resonators with PT-symmetry especially when the system's refractive index obeys $n(x) = n^*(x)$ where x is a coordinate in the system [11], [21]–[23]. One way of transforming the eigenvalues of a PT-symmetric system, which is being valued to be complex, is by tuning one of the system variables, e.g., frequency, gain and loss parameters, coupling, etc., and the resultant transition point is an EPD [22], [24], [25]. Notably, systems displaying only loss (either through dissipative mechanisms or via radiation leakage) may also exhibit EPDs [20], [26].

The attainment of EPDs occurs when the matrix of the system has the Jordan block or is composed of it [27]–[29]. The representation of the eigenstate at the EPD occurs through the eigenvectors that are generalized instead of having the regular eigenvectors [27], [30]. These contribute to the algebraic system eigenstates growth [27], [29]. Due to EPDs being rare, they can only be found or engineered in numerous structures because of their useful nature to conceive a variety of devices. Examples of applications include active systems gain [18], [31]–[35], enhanced sensors [1], [2], [36], and antennas directivity among others [37]. This dissertation will examine a third order EPD conditions in coupled RLC resonators which

can be used as an extremely sensitive sensor due to the sensitivity to the perturbations of the system at the third order EPD.

Sec. 1.2 The Source Free Parallel RLC Oscillator:

As our proposed third order EPD coupled resonators will basically rely on the well known parallel RLC oscillator, we ought to briefly point out its features. To obtain these features we will use the state variable method as it will become very useful when we analyze the third order EPD coupled RLC resonators.

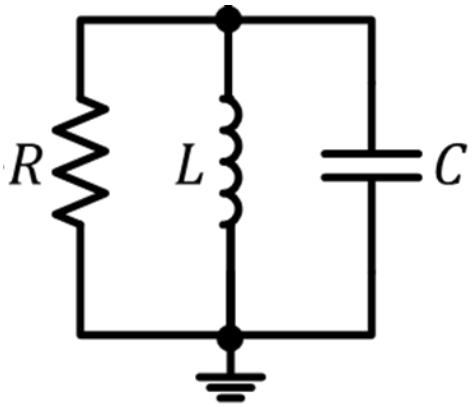

Figure 1: The source free parallel RLC oscillator

1.2.1: State Variable Analysis:

There are several methods by which circuits might be analyzed. Here, we analyze circuits in their time domain and by using the state-variable analysis or often referred to as "state space analysis." Generally, the state-variable method can show the dynamics as setoff coupled first-order differential equations expressed as a linear combination of all state variables [38]. In state variable analysis, it is appropriate to select capacitor voltages and inductor currents as a hybrid set. The energy stored in inductors and capacitors can be

expressed using the set of variables. Accordingly, the system's energy state can be described by capacitor voltages and inductor currents. Therefore, the quantities are referred to as "state variables."

In order to construct a set of normal-from equations (the derivative of the state variable is expressed as a linear combination of all the state variables) of the RLC oscillator in Figure 1, (Ch. 19 in [39]) suggests the following:

- The first step is to establish a normal tree. In this step, voltage sources and capacitors are placed in the tree. The cotree, on the other hand, should contain current sources and inductors. The resistor current will be represented by the capacitor voltage divided by the resistance. So, it should be placed in the cotree. Figure 1 will then be transformed to the normal tree shown in Figure 2. The solid line is to represent the voltage across the capacitor and the dashed lines are representing the flow of the currents chosen here to be downward.

-

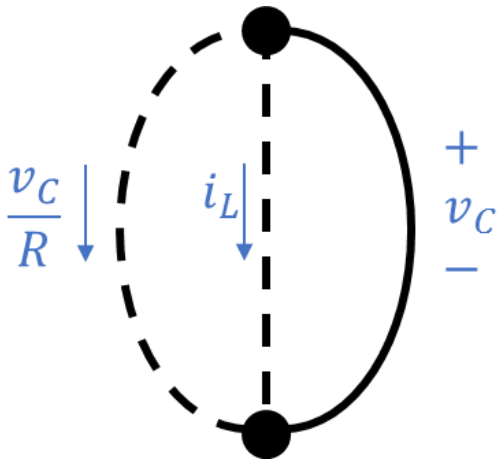

- Figure 2: Normal tree of the source free RLC oscillator. Solid line is the voltage across the capacitor and dashed lines are the current through the inductor and the resistor.

- The next step involves writing the C equation. Generally, we use KCL to write a single equation for every capacitor in the circuit. Afterward, set $C\frac{dv_C}{dt}$ to be equal to the total link currents. So, the first order equation representing the capacitor is obtained by applying KCL to the top central node:

$$\frac{dv_C}{dt} = -\frac{1}{CR}v_C - \frac{1}{C}i_L \tag{1.1}$$

- The third step is about writing the L equation. Similarly, KVL can be used to derive the expressions for all inductors in the circuit. set $L\frac{di_L}{dt}$ to be equal to the sum of tree-branch voltages derived when the single closed path is taken into account. The path to be considered consists of the branches and links where the inductors are located. So, the first order equation representing the inductor is obtained by applying KVL to the right loop:

$$\frac{di_L}{dt} = \frac{1}{L}v_C \tag{1.2}$$

- The last step is to write the non-formal equations which are equations (1.1) and (1.2) as.

$$\begin{aligned} \frac{dv_C}{dt} &= -\frac{1}{CR}v_C - \frac{1}{C}i_L \\ \frac{di_L}{dt} &= \frac{1}{L}v_C \end{aligned} \tag{1.3}$$

To obtain the characteristic equation of the parallel RLC oscillator, we express (1.3) and using the matrix notation which will also be used in analyzing the third order EPD system. In general, this approach is useful as the number of variables rises with an increase in the number of capacitors and inductors in a circuit. So, we represent the normal-form equations in (1.3) by a matrix equation in which the state vector that contains all the state variables is defined as $\mathbf{\Psi}(t) = \begin{bmatrix} v_C & i_L \end{bmatrix}^T$, where T denotes the transpose operator. The matrix equation will be

$$\frac{d\mathbf{\Psi}}{dt} = \underline{\mathbf{M}}\mathbf{\Psi}(t) \tag{1.4}$$

The solutions of the equation (1.4) is assumed to be of the form $e^{\lambda t}$. We can construct the eigenvalue problem as

$$(\underline{\mathbf{M}} - \lambda \underline{\mathbf{I}})\mathbf{\Psi} = \mathbf{0} \tag{1.5}$$

where λ_k with $k = 1, 2$ are the eigenvalues of the 2 × 2 system matrix $\underline{\mathbf{M}}$ that is constructed as

$$\underline{\mathbf{M}} = \begin{bmatrix} -\dfrac{1}{RC} & -\dfrac{1}{C} \\ \dfrac{1}{L} & 0 \end{bmatrix} \tag{1.6}$$

The eigenvalues of $\underline{\mathbf{M}}$ can be obtained from the characteristic equation of $\underline{\mathbf{M}}$ by setting $\det(\underline{\mathbf{M}} - \lambda \underline{\mathbf{I}})$ to zero. The characteristic equation of the RLC oscillator is

$$\lambda^2 + \frac{1}{RC}\lambda + \frac{1}{LC} = 0 \tag{1.7}$$

where the eigenvalues λ are the roots of (1.7). The roots of the characteristic equation are

$$\lambda_{1,2} = -\frac{1}{2RC} \pm \sqrt{\left(\frac{1}{2RC}\right)^2 - \frac{1}{LC}} \quad \text{or} \quad \lambda_{1,2} = -\alpha \pm \sqrt{\alpha^2 - \omega_o^2} \tag{1.8}$$

where $\alpha = \frac{1}{2RC}$ is the damping factor or the loss/gain parameter as we will call it in the next chapters and $\omega_o = \frac{1}{\sqrt{LC}}$ is the resonant frequency of the RLC oscillator. The associate eigenvectors of the matrix $\underline{\mathbf{M}}$ are $\mathbf{\Psi}_n = \begin{bmatrix} \frac{-1}{C} & \lambda_{1,2} + \frac{1}{RC} \end{bmatrix}^T$, $n = 1, 2$. From the eigenvectors expression, we observe that degenerate eigenvalues lead the eigenvectors to coalesce which indicates a second order EPD. This EPD will cause critically damped modes of the RLC oscillators. In the rest of the Thesis we investigate higher order degeneracies that do not exhibit critical damping, i.e., they may have purely imaginary eigenvalues (purely real resonant frequencies).

Sec. 1.3 Negative Resistance:

Negative resistance is a regular resistor with a negative value such that the device obeys Ohm's law but the current flows backwards (from low voltage to high voltage). The I-V curve for such device has negative slope. A passive device displaying these properties violate the principles of conservation of energy. Therefore, when we refer to a negative resistor in the next chapters as $-R$, we assume that it is obtained using active devices. One way to obtain negative resistance is using the so called negative impedance convertor (NIC) shown in Figure 3.

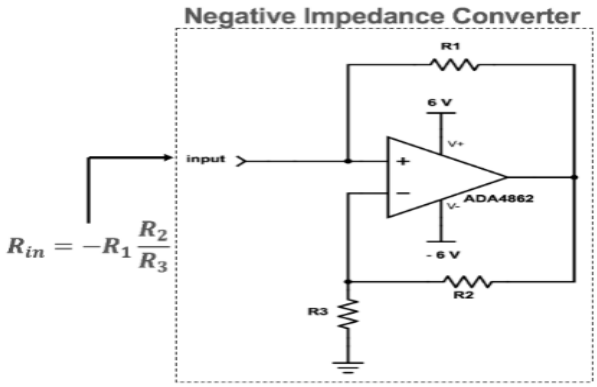

Figure 3: Negative impedance convertor as one example to represent a negative resistor.

Sec. 1.4 Organization of the thesis and contents:

The thesis is organized into Chapters that involve the theory and validations of the third order EPD in the coupled resonators.

Chapter 2. We introduce in this chapter the third order EPD coupled resonators and their configuration. Furthermore, we also present the state variables of the coupled resonators and their corresponding normal-from equations. We further establish the characteristic equation of the system which we use to plot the dispersion diagram.

Chapter 3. In this chapter, two methods are presented to validate the existence of a third order EPD by examining the system eigenvectors. The first method is called hyperdistance which indicates a third order EPD as it goes to zero. The second is to use the magnitude of the complex correlation coefficient as indication of coalescence.

Chapter 4. We analyze the coupled resonators time domain response by finding the explicit time domain functions of the state variables. We further show the simulation results of the modes at the 3rd order EPD and normal condition.

CHAPTER 2

THIRD ORDER EPD COUPLED RESONATORS

Sec. 2.1 The Configuration of the Third Order EPD Coupled Resonators:

In this section, we introduce the third order EPD coupled resonators and its configuration. It consists of an LC tank associated with C_a and L_a which is coupled with the pair coupled RLC oscillators (similar to the RLC oscillators discussed in Sec. 1.1) and the whole configuration is shown in Figure 4. In this figure, C_{c_3} is used to couple the two RLC oscillators and R_1 here represents a negative resistance $-R$ which provides linear amplification, i.e. gain as discussed in Sec. 1.3. Note that in practical configuration there must more than one $-R$ to compensate for the coil loss in the inductors to maintain oscillations. Whereas R_2 represents linear attenuation with equal amount to R, i.e. loss. A two coupled RLC oscillators one with gain and the other with equal loss are an ideal PT-symmetry dimer, studied in [13], where a breaking point between the exact and "broken phase" was shown and defined as PT-symmetry breaking point which is also an example of a second order EPD as we will see in Sec. 2.2. Here, C_{c_1} and C_{c_2} couple the additional LC tank to the RLC resonator with gain and RLC resonator with loss, respectively. Another way to couple the resonators is

to use mutual coupling, i.e. to couple the inductors instead of the capacitance coupling. For simplicity, we only used capacitance coupling connecting the nodes as shown in Figure 4.

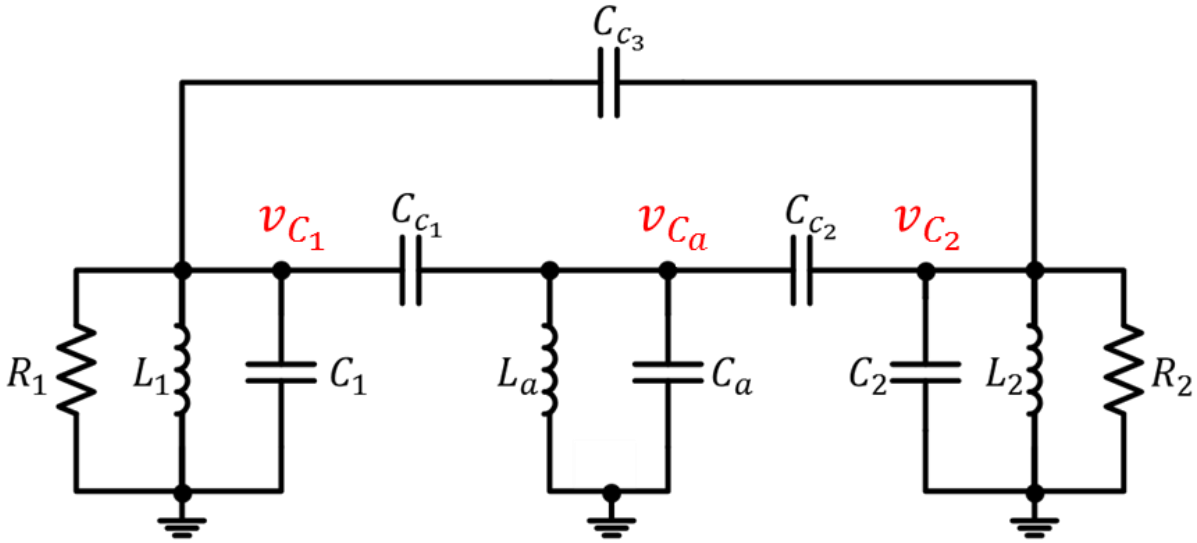

Figure 4: The proposed third order EPD coupled resonators and coupling mechanism with capacitances.

Sec. 2.2 The Multidimensional First Order Differential Equation:

This section analyzes the normal mode dynamics of this 3rd order EPD coupled resonators. To obtain the normal-form equations of the coupled resonators in which we use to construct the multidimensional first-order differential equation (the matrix equation), the state variable method discussed in Sec. 1.2.1 is used. We start by drawing the tree diagram of the coupled resonators, shown in Figure 5. KCL is used at the top three nodes of Figure 5 to obtain $\frac{dv_{C_1}}{dt}$, $\frac{dv_{C_a}}{dt}$, and $\frac{dv_{C_2}}{dt}$ equations while considering the assigned polarity references for the voltages and assigned direction for the current.

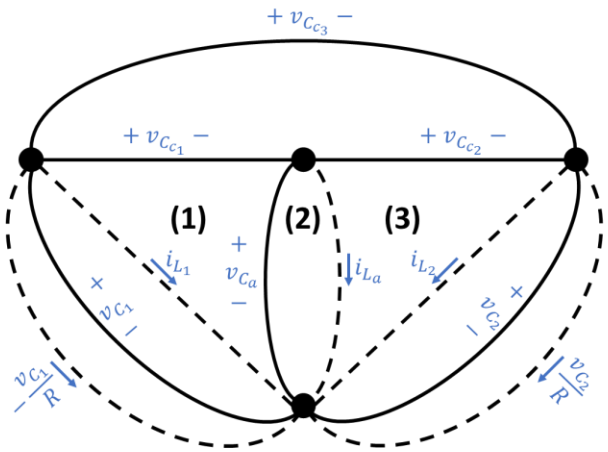

Figure 5: Normal tree of the third order EPD coupled resonators showing the state variables. Solid lines are the voltage across the capacitors and dashed lines are the current through the inductors and the resistors.

KVL is then used in loops (1), (2), and (3) in Figure 5 to obtain $\frac{di_{L_1}}{dt}$, $\frac{di_{L_a}}{dt}$, and $\frac{di_{L_2}}{dt}$ respectively. We finally consider that

$$v_{C_{c_1}} = v_{C_1} - v_{C_a} \tag{2.1}$$

$$v_{C_{c_2}} = v_{C_a} - v_{C_2} \tag{2.2}$$

$$v_{C_{c_3}} = v_{C_1} - v_{C_2} \tag{2.3}$$

For simplicity, all capacitors are chosen to be equal to C. For a balanced loss and gain, L_1 and L_2 must be equal [13], i.e., $L_1 = L_2 = L$, and also $R_1 = -R_2 = -R$. We then can redraw the coupled resonators in Figure 4 taking into account those values of the different parameters as in Figure 6.

The state variables have been arbitrary ordered as v_{C_1}, v_{C_a}, v_{C_2}, i_{L_1}, i_{L_a}, and i_{L_2}. The six normal-form equations are

$$\frac{dv_{C_1}}{dt} = \alpha v_{C_1} - 0.5\alpha v_{C_2} - \frac{1}{2C} i_{L_1} - \frac{1}{4C} i_{L_a} - \frac{1}{4C} i_{L_2}$$

$$\frac{dv_{C_a}}{dt} = 0.5\alpha v_{C_1} - 0.5\alpha v_{C_2} - \frac{1}{4C} i_{L_1} - \frac{1}{2C} i_{L_a} - \frac{1}{4C} i_{L_2}$$

$$\frac{dv_{C_2}}{dt} = 0.5\alpha v_{C_1} - \alpha v_{C_2} - \frac{1}{4C} i_{L_1} - \frac{1}{4C} i_{L_a} - \frac{1}{2C} i_{L_2}$$

$$\frac{di_{L_1}}{dt} = \frac{1}{L} v_{C_1} \tag{2.4}$$

$$\frac{di_{L_a}}{dt} = \frac{1}{L_a} v_{C_a}$$

$$\frac{di_{L_2}}{dt} = \frac{1}{L} v_{C_2}$$

where $\alpha = \frac{1}{2RC}$ is the loss/gain parameter.

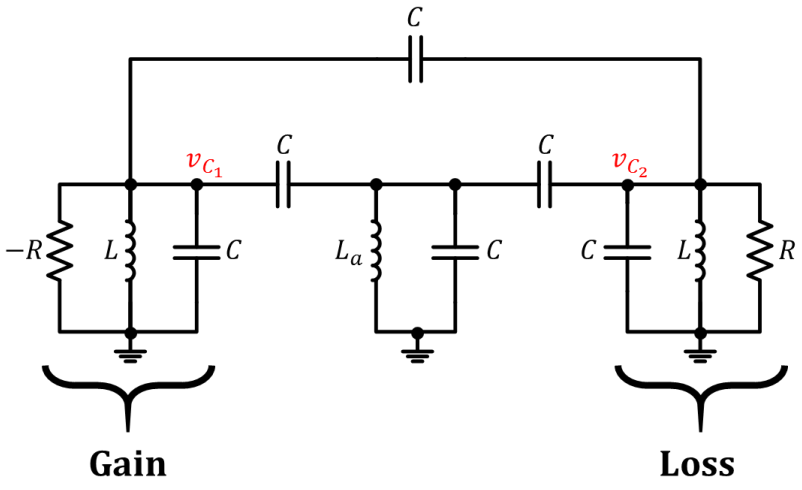

Figure 6: The simplified third order coupled resonators showing loss and gain. For some value of *R* this circuits shows a third order EPD.

As discussed in Sec. 2.1, EPD can be observed when the eigenfrequencies and eigenmodes of the system coalesce. One method to obtain the eigenfrequencies and eigenmodes is discussed in Sec. 1.2.1 namely the state variable method. We define the state vector that contains all the state variables as $\mathbf{\Psi}(t)=\begin{bmatrix} v_{C_1} & v_{C_a} & v_{C_2} & i_{L_1} & i_{L_a} & i_{L_2} \end{bmatrix}^T$, where T denotes the transpose operator. The time evolution of the state vector obeys the multidimensional first-order differential equation

$$\frac{d\mathbf{\Psi}}{dt}=\underline{\mathbf{M}}\mathbf{\Psi}(t) \tag{2.5}$$

where $\underline{\mathbf{M}}$ is the 6 × 6 system matrix. From the normal-form equations in (2.4), we construct the system matrix and the state vector as

$$\underline{\mathbf{M}}=\begin{bmatrix} \alpha & 0 & -\frac{\alpha}{2} & -\frac{1}{2C} & -\frac{1}{4C} & -\frac{1}{4C} \\ \frac{\alpha}{2} & 0 & -\frac{\alpha}{2} & -\frac{1}{4C} & -\frac{1}{2C} & -\frac{1}{4C} \\ \frac{\alpha}{2} & 0 & -\alpha & -\frac{1}{4C} & -\frac{1}{4C} & -\frac{1}{2C} \\ \frac{1}{L} & 0 & 0 & 0 & 0 & 0 \\ 0 & \frac{1}{L_a} & 0 & 0 & 0 & 0 \\ 0 & 0 & \frac{1}{L} & 0 & 0 & 0 \end{bmatrix} \tag{2.6}$$

$$\mathbf{\Psi}(t)=\begin{bmatrix} v_{C_1} & v_{C_a} & v_{C_2} & i_{L_1} & i_{L_a} & i_{L_2} \end{bmatrix}^T \tag{2.7}$$

We can observe the behavior of the eigenfrequencies and eigenmodes of such a system when the loss/gain parameter (α) changes through finding the eigenvalues of the system matrix

$\underline{\mathbf{M}}$. Assuming solutions of the equation (2.5) of the form $\boldsymbol{\Psi} \propto e^{\lambda t}$, we can construct the eigenvalue problem as

$$\left(\underline{\mathbf{M}} - \lambda \underline{\mathbf{I}}\right)\boldsymbol{\Psi} = \mathbf{0} \tag{2.8}$$

where λ_k with $k = 1, 2, \ldots, m$ and m is the order of the matrix, $m = 6$ in this case, are the eigenvalues of the system matrix $\underline{\mathbf{M}}$. Assuming a time varying convention $e^{j\omega t}$, the complex system eigenfrequencies ω_k are related to the eigenvalues as $\lambda_k = j\omega_k$. The eigenvalues of $\underline{\mathbf{M}}$ can be obtained by finding the roots of the characteristic equation $\det\left(\underline{\mathbf{M}} - \lambda \underline{\mathbf{I}}\right) = 0$. Upon expanding the determinant of the system matrix, we evidently get a 6th order polynomial equation of the from

$$\lambda^6 + \left(\frac{L + 2L_a}{2CLL_a} - \frac{3}{4}\alpha^2\right)\lambda^4 + \left(\frac{6L + 3L_a - 4CL^2\alpha^2}{16C^2L^2L_a}\right)\lambda^2 + \frac{1}{16C^3L^2L_a} = 0 \tag{2.9}$$

By the fundamental theorem of algebra, this polynomial (2.9) has 6 roots. Since all the coefficients are real, the roots must be either real or complex conjugate pairs. Thus, a 6 × 6 matrix has 6 eigenvalues where we can have repeated eigenvalues. Repeated eigenvalues of $\underline{\mathbf{M}}$ is desired in order to obtain EPD.

Sec. 2.3 Exceptional Point of Degeneracy (EPD) in the Coupled Resonators:

The EPD is the point in parameter space (like in a dispersion diagram) where because of loss/gain in the coupled resonators, the system matrix $\underline{\mathbf{M}}$ in (2.6) is not diagonalizable and

is similar to a matrix that contains one or more Jordan blocks. As discussed in Sec. 1.2, EPD occurs due to the coalescence of system eigenstates in both their eigenvalues and *eigenvectors* which will form a degenerate eigenvector, i.e., the point at which the algebraic multiplicity of an eigenvalue is larger than its geometrical multiplicity. Algebraic multiplicity of an eigenvalue is defined in Ch. 5 of [40] as the number of repetition of that eigenvalue, denoted by p and the geometric multiplicity as the number of the linearly independent eigenvectors associated with that eigenvalue, denoted by l. In this Thesis we consider a third order EPD which indicates an algebraic multiplicity of the eigenvalues $p=3$ and their geometric multiplicity $l=1$. We show that this is obtained by properly coupling three resonators with loss and gain.

2.3.1: Necessary Condition for the Third Order EPD:

At the third order EPD frequency, the characteristic dispersion equation of the system can be simply arranged since the coupled resonators has two repeated eigenvalues of multiplicity 3 which must appear in complex conjugate pair. Therefore, the characteristic equation in (2.9) at the third order EPD must have the following form

$$\left(\lambda-\lambda_e\right)^3\left(\lambda-\lambda_e^*\right)^3=0 \tag{2.10}$$

where the symbol $*$ denotes the complex conjugate and $\lambda_e=\lambda_r+j\lambda_i$ is the eigenvalue of the system matrix $\underline{\mathbf{M}}$. The third order EPD eigenfrequency ω_e is equal to $-j\lambda_e$. The characteristic equation (2.9) and the general dispersion equation (2.10) are both sixth order

polynomials. By equating and simplifying the coefficients of different powers of λ, we obtain the three following equations:

$$6CLL_a\lambda_i^2 - L - 2L_a + \frac{3CLL_a}{2}\alpha^2 = 0$$

$$48C^2L^2L_a\lambda_i^4 - 6L + 3L_a + 4CL^2\alpha^2 = 0 \qquad (2.11)$$

$$16C^3L^2L_a\lambda_i^6 - 1 = 0$$

Coupled resonators parameters of a system which exhibit a third order EPD must satisfy these equations. These are the necessary (but not sufficient) conditions of the different coupled resonators parameters that grant the occurrence of a third order degeneracy of eigenvalues in the described system [41].

Sec. 2.4 Dispersion Using the State Variable Method:

We solve the three necessary equations in (2.11) for third order EPD numerically by assuming some values for C and L such that the coupled resonators can operate at radio frequencies. We then obtain the values of λ_i, L_a, and α at which the 3rd order EPD of the system occurs; i.e., the characteristics equation (2.9) will have two repeated roots of multiplicity 3. We denote α obtained from solving (2.11) by α_e which indicates the gain/loss parameter at which 3rd EPD exists. When we assume $C = 330\,\text{pF}$ and $L = 10\,\mu\text{H}$, we get $L_a \approx 12\,\mu\text{H}$, and $\alpha_e = 10.9\times10^4\,\frac{\text{S}}{\text{F}}$.

We plug in these parameters into the system matrix $\underline{\mathbf{M}}$ to obtain the eigenvalues and plot the dispersion diagram. Figure 7 illustrates the dispersion diagram of the normalized eigenfrequencies ω_k / ω_o of $\underline{\mathbf{M}}$ where $\omega_o = \frac{1}{\sqrt{LC}} = 17\ \text{Mrad/s}$, versus the normalized gain/loss parameter α / α_e. The six eigenfrequencies come in two sets of positive-negative pairs, each set containing three eigenfrequencies.

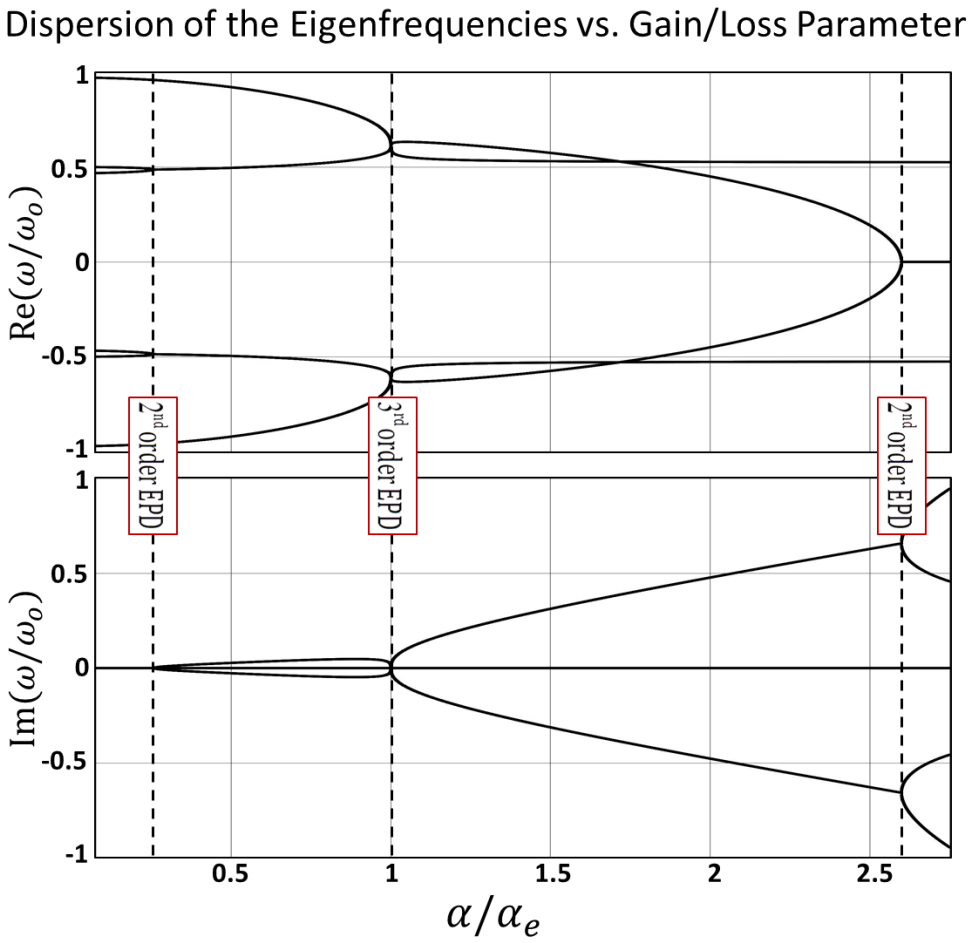

Figure 7: Dispersion diagram of the real and imaginary parts of the eigenfrequencies versus the gain/loss parameter of the RLC coupled resonators. The three dashed lines indicate three EPD points. The first and last EPDs are EPDs of second order and the middle one is the desired third order EPD.

In Figure 7, we identify three special points, shown with dashed vertical lines. The first point as α/α_e increases, is a 2nd order EPD which we will define as $\hat{\alpha}_1$ (an algebraic multiplicity of the eigenvalues $p=2$). The second point is the desired 3rd order EPD occurring at $\alpha=\alpha_e$ (an algebraic multiplicity of the eigenvalues $p=3$). Finally, we observe the third point which is another 2nd order EPD and is defined as $\hat{\alpha}_2$ (an algebraic multiplicity of the eigenvalues $p=2$).

In the region of $0<\alpha/\alpha_e<\hat{\alpha}_1$, the six eigenfrequencies are purely real. Considering the these purely real eigenfrequencies, the solutions of the state variables are just oscillatory (we will elaborate more on this in the time domain section in Ch. 4). This interval can be compared to the "exact phase" seen in [13] since the modes here are "exactly" PT-symmetric where it can be shown that the time varying v_{C_1} and v_{C_2} responses are symmetric.

While in the two regions of $\hat{\alpha}_1<\alpha/\alpha_e<\hat{\alpha}_2$ (excluding when $\alpha=\alpha_e$), there complex conjugate eigenfrequencies. Due to the existence of real and imaginary eigenfrequencies, there modes are exponentially growing and exponentially decaying that oscillate at the same frequencies. This region can also be referred to as "broken phase".

The final region observed is when $\hat{\alpha}_2<\alpha/\alpha_e$. Here, this region is similar to the aforementioned region where we observe complex conjugate eigenfrequencies. Note, the branching point at $\hat{\alpha}_2$ is a second order EPD.

The time domain responses of the state variables at these special points will be discussed in Sec. 4.3. To validate the dispersion diagram in Figure 7, we create another sixth

order polynomial equation in which its roots are the eigenfrequencies of the coupled resonators. This is possible by using the transverse resonance method which we will explain in the next section.

Sec. 2.5 Dispersion Using the Transverse Resonance Method:

The transverse resonance technique which originated as an application of the microwave circuits formalism in the longitudinal direction to the actual power flow in a cylindrical waveguide [42]. It has then been widely used in waveguides to solve the dispersion relation for the dominant mode [43]. We use this technique here to solve for the coupled resonators frequency response. This method does not depend on the state variables, instead it only analyzes the impedances (admittance) of the whole coupled resonators. The approach is to split the coupled resonators in Figure 6 into two parts (left part and right part) with each part conserving its own equivalent impedance Z_k or admittance Y_k with k indicating each side (L for left or R for right). Adding the two impedances (admittances) and equating them to zero will provide a 6^{th} order polynomial equation. The roots of this polynomial equation are the eigenfrequencies of the system which can be compared to the eigenfrequencies obtained in Sec. 2.3.

Breaking the circuit of Figure 6 into two parts (left and right parts) will results in finding the impedances (admittances) of a three-terminals circuit. An easier way for obtaining two terminal circuit when broken into two parts to calculate the equivalent impedances (admittances) of each part is to transfer the delta configuration containing the three coupling capacitors C_{c_1}, C_{c_2}, and C_{c_3} into a Y configuration as shown in Figure 8. The

three capacitors in the delta configuration are assumed to be equal to C which results in C_y being three times larger than C since

$$C_y = \frac{CC + CC + CC}{C} = 3C \tag{2.12}$$

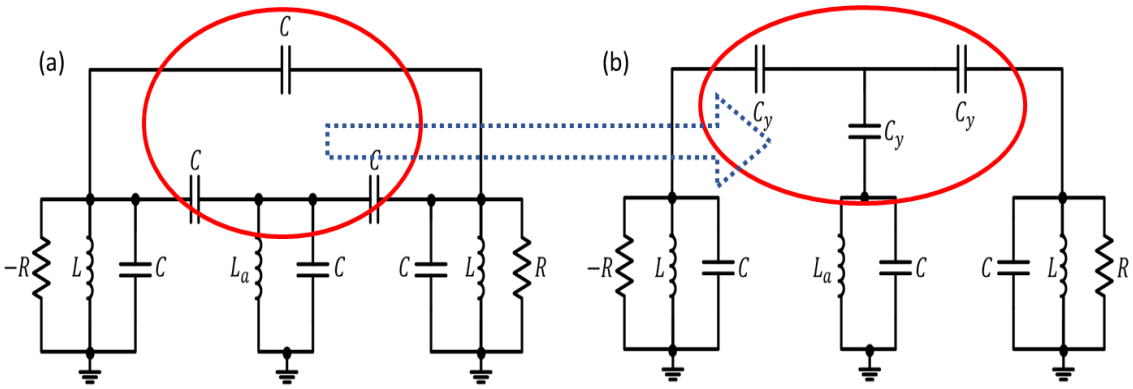

Figure 8: (a) The original coupled resonators showing the delta configuration. (b) Thee transformed coupled resonators showing the Y configuration.

Figure 9 demonstrates the left and right parts of the circuit in Figure 8 (b) with Y_L and Y_R corresponding to the total admittance of the left and right parts respectively. The frequency response of the circuit is obtained by solving

$$Y_L + Y_R = 0 \tag{2.13}$$

Equation (2.13) is a 6th order polynomial equation consisting of a single variable ω and some complex coefficients caused by the admittance of the capacitors and inductors as they are purely imaginary.

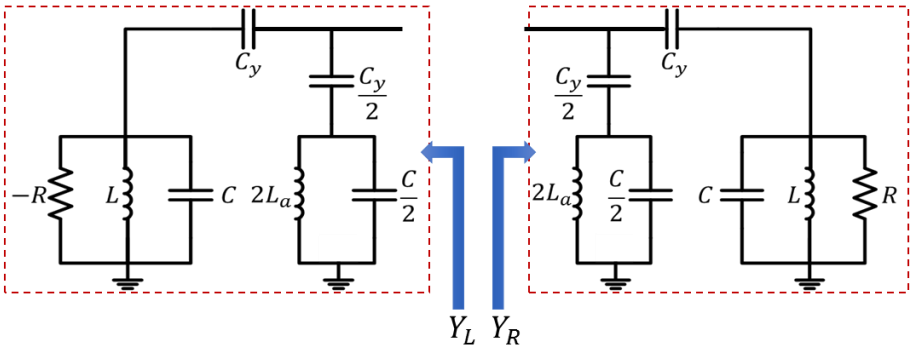

Figure 9: The right and Left parts of the circuit with their equivalent admittances.

We solve for the roots of equation (2.13) which correspond to the complex frequencies of the coupled resonators. Then, we compare these complex frequencies with the eigenfrequencies obtained in Sec. 2.3. A comparison of two methods dispersion diagram of the real and imaginary frequencies versus the gain/loss parameter is shown in Figure 10. As expected, there is an excellent agreement of the two methods.

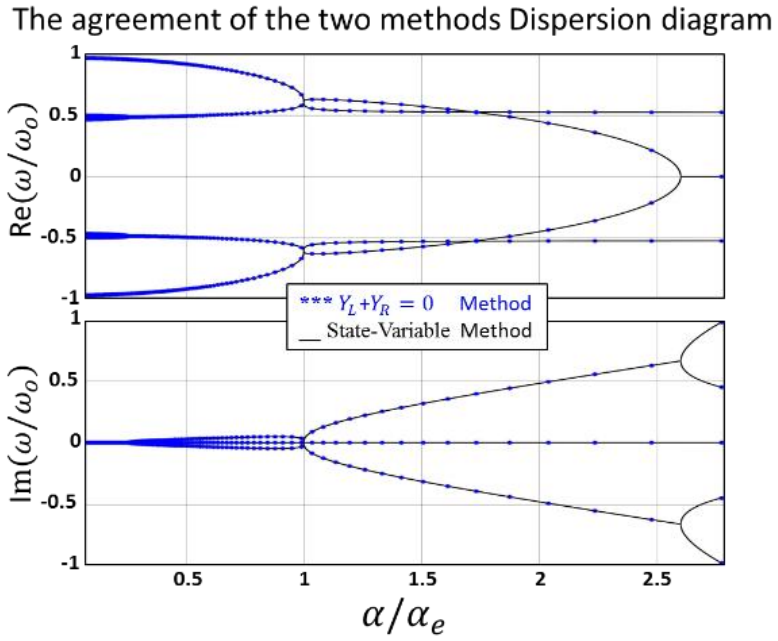

Figure 10: Comparison of state variable and transverse resonance methods dispersion diagram. Black colored line is the dispersion diagram obtained in Sec. 2.4. The agreement of the two results is shown.

Sec. 2.6 Summary:

In this chapter, we have demonstrated the configuration of the third order EPD coupled resonators. We have shown the use of the state variable method to construct the multidimensional differential equation which represents the state vector containing the state variables i.e. the voltages and currents of the capacitors and inductors respectively in the time domain. We have also presented the dispersion diagram of the eigenfrequencies of the coupled resonators versus the loss/gain parameter where three special points were shown. Two of these three special points are second order EPDs and the third one is a third order EPD. We finally used the transverse resonance method to obtain the dispersion diagram and compare it with the aforementioned diagram in which we showed the two methods produced the same dispersion as expected.

CHAPTER 3

VALIDATION OF THE OCCURANCE OF THIRD ORDER EPD

In Ch. 2, we observed the existence of a third order EPD by investigating the behavior of the eigenfrequencies. However, EPD occurrence is only confirmed at degenerate resonance frequencies where multiple eigenmodes (i.e. the eigenvectors of $\underline{\mathbf{M}}$) of the system coalesce. Noteworthy is that coalescing of all the independent eigenvectors result in the third order EPD. It is necessary for an individual to examine the quality of the EPD states that can undergo any design of perturbation, including losses, the tolerance of the parameters or a possible frequency detuning. Therefore, it becomes essential to incorporate qualitative validations that enable the observation of precise exceptional points of degeneracy (EPD). We use two figures of merits for the numerical validation of the third order EPD.

Sec. 3.1 Hyperdistance:

The first figure of merit we use is defined in [44] as the development of the concept of hyperdistance $D_H(\omega)$ among all the eigenvectors of the system matrix $\underline{\mathbf{M}}$ to establish the closeness to an EPD. In [44], they developed this method to investigate the occurrence of a degenerate band edge (DBE) which is an example of a fourth order EPD. For our purpose, we define the hyperdistance for the third order EPD as

$$D_H = \frac{1}{60} \sum_{\substack{m=1,n=1,l=1 \\ m\neq n\neq l}}^{6} \left(\sin\left(\theta_{mn}\right) + \sin\left(\theta_{ml}\right) + \sin\left(\theta_{nl}\right)\right) \tag{3.1}$$

where for two general vectors, $\mathbf{\Psi}_m, \mathbf{\Psi}_n$, the angle between the two vectors, θ_{mn}, in three-dimensional complex vector space is define as

$$\theta_{mn} = \cos^{-1}\left(\frac{\mathrm{Re}\left(\mathbf{\Psi}_m \cdot \mathbf{\Psi}_n\right)}{\left\|\mathbf{\Psi}_m\right\|\left\|\mathbf{\Psi}_n\right\|}\right) \tag{3.2}$$

where $\cdot$ is the scalar product of two vectors and $\left\|\mathbf{\Psi}_n\right\|$ represents the norm of the vector. When the coupled resonators undergo a third order EPD, it indicates that all the eigenvectors in the matrix system are coalesced. As a result, the Figure of Merit (FOM) will automatically attain a hyperdistance that is identically equivalent to zero. It is essential to note, when losses or perturbation of parameters are added, the proposed figure of merit is always not zero at the frequency of the third order EPD. It is important to assume that the EPD emerge practically when the FOM is significantly at a minimum value. This happens regardless of the precision of the third order EPD as a mathematical condition that is feasible in ideal lossless using numerical techniques. We illustrate this concept in Figure 11 where we plot the hyperdistance obtained from (3.1) for different values of the gain/loss parameter α. The real frequencies of the system are also plotted as a reference for the location of the EPD points. The blue line in Figure 11 represent the $\left|\det\left(\underline{\mathbf{U}}\right)\right|$ used for comparison purposes. Where $\underline{\mathbf{U}}$ is a 6×6 matrix containing the six eigenvectors of $\underline{\underline{\mathbf{M}}}$ in its columns namely $\underline{\mathbf{U}} = \left[\mathbf{\Psi}_1 \middle| \mathbf{\Psi}_2 \middle| \mathbf{\Psi}_3 \middle| \mathbf{\Psi}_4 \middle| \mathbf{\Psi}_5 \middle| \mathbf{\Psi}_6\right]$.

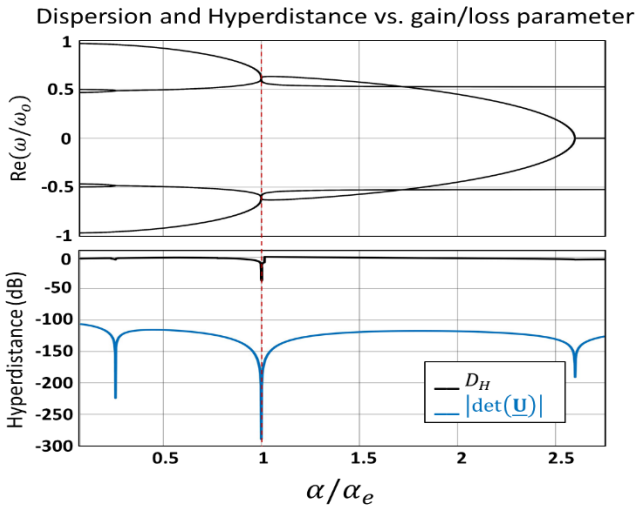

Figure 11: Dispersion relation of the real frequency compared with hyperdistance as the normalized gain/loss parameter increases. The blue line is the $\left|\det\left(\underline{\mathbf{U}}\right)\right|$ used to show all the EPD points. The hyperdistance provides the validation of the 3rd order EPD since it is minimum only at that location.

EPDs occur at the minimum value of $\left|\det\left(\underline{\mathbf{U}}\right)\right|$. However, the third order EPD (when $\alpha = \alpha_e$) can only be observed by monitoring the minimum value of the hyperdistance D_H as seen in Figure 11. This technique validated the existence of the third order EPD although the minimum value of D_H was not as low as the minimum value of $\left|\det\left(\underline{\mathbf{U}}\right)\right|$, but it was significantly at minimum value at desired EPD compared to its other value.

Sec. 3.2 Complex Correlation Coefficient:

The second figure of merit proposed here is to use a well-known method in statistics namely the Pearson product-moment correlation coefficient. This method was developed by Karl Pearson during the end of the nineteenth century [45] and has been widely used since then. The Pearson product-moment correlation coefficient is commonly referred to as Pearson's correlation or simply as the correlation coefficient and it is dimensionless and

denoted by ρ. It is a value between -1 and 1 that summarizes the closeness of linear relations between two real variables. A correlation coefficient of zero indicates the two real variables are not related. A correlation coefficient value of 1 indicates that for every positive rise in one real variable, the other real variable will also rise of a fixed proportion. Similarly. When a -1 correlation coefficient means for every positive rise in one real variable, there is a negative decay of a fixed proportion in the other real variable.

Here we compare the correlation of the eigenvectors shown in matrix $\underline{\mathbf{U}}$. However, these eigenvectors are not real, they are usually complex instead which will result in a complex correlation coefficient ρ. The correlation coefficient of complex sequences is widely used and has an important role in array signal processing [46]. Another application where the complex correlation coefficient is utilized is in Synthetic Aperture Radar (SAR) in which the magnitude and the phase of the complex correlation coefficient are used to compare and combine the information of two images [47]. The complex correlation coefficient between two eigenvectors $\mathbf{\Psi}_m$ and $\mathbf{\Psi}_n$ is defined as

$$\rho_{\mathbf{\Psi}_m \mathbf{\Psi}_n} = \frac{\mathrm{Cov}[\mathbf{\Psi}_m, \mathbf{\Psi}_n]}{\mathrm{Std}[\mathbf{\Psi}_m]\mathrm{Std}[\mathbf{\Psi}_n]} \tag{3.3}$$

where $\mathrm{Cov}[\mathbf{\Psi}_m, \mathbf{\Psi}_n]$ is the covariance between the two eigenvectors $\mathbf{\Psi}_m$ and $\mathbf{\Psi}_n$, and $\mathrm{Std}[\mathbf{\Psi}]$ is the standard deviation of the eigenvector $\mathbf{\Psi}$ which can be calculated respectively by

$$\mathbf{Cov}[\mathbf{\Psi}_m, \mathbf{\Psi}_n] = \frac{\sum_{k=1}^{L} \left(\mathbf{\Psi}_m[k] - \overline{\mathbf{\Psi}_m}\right)\left(\mathbf{\Psi}_n[k] - \overline{\mathbf{\Psi}_n}\right)^*}{L-1} \tag{3.4}$$

$$\mathrm{Std}[\boldsymbol{\Psi}] = \sqrt{\frac{\sum_{k=1}^{L}\left(\boldsymbol{\Psi}[k]-\overline{\boldsymbol{\Psi}}\right)\left(\boldsymbol{\Psi}[k]-\overline{\boldsymbol{\Psi}}\right)^{*}}{L-1}} \tag{3.5}$$

with L being the length of the eigenvector and $\overline{\boldsymbol{\Psi}} = \frac{1}{L}\sum_{k=1}^{L}\boldsymbol{\Psi}[k]$ which is the average of eigenvector $\boldsymbol{\Psi}$. We combine (3.3), (3.4), and (3.5) to obtain the final formula of the complex correlation coefficient as a function of any two eigenvectors presented in $\underline{\mathbf{U}}$ to be equal to

$$\rho_{\boldsymbol{\Psi}_m\boldsymbol{\Psi}_n} = \frac{\sum_{k=1}^{6}\left(\boldsymbol{\Psi}_m[k]-\overline{\boldsymbol{\Psi}_m}\right)\left(\boldsymbol{\Psi}_n[k]-\overline{\boldsymbol{\Psi}_n}\right)^{*}}{\sqrt{\sum_{k=1}^{6}\left(\boldsymbol{\Psi}_m[k]-\overline{\boldsymbol{\Psi}_m}\right)\left(\boldsymbol{\Psi}_m[k]-\overline{\boldsymbol{\Psi}_m}\right)^{*}}\sqrt{\sum_{k=1}^{6}\left(\boldsymbol{\Psi}_n[k]-\overline{\boldsymbol{\Psi}_n}\right)\left(\boldsymbol{\Psi}_n[k]-\overline{\boldsymbol{\Psi}_n}\right)^{*}}} = \left|\rho_{\boldsymbol{\Psi}_m\boldsymbol{\Psi}_n}\right| e^{j\theta}$$

(3.6)

where $m = 1,2,\ldots,5$, $n = 2,3,\ldots,6$, and $m \neq n$ in our system. Note that $0 \leq \left|\rho_{\boldsymbol{\Psi}_m\boldsymbol{\Psi}_n}\right| \leq 1$. Although, the magnitude of the complex correlation coefficient $\left|\rho_{\boldsymbol{\Psi}_m\boldsymbol{\Psi}_n}\right|$ by itself does not necessarily provide valuable insight on the relation between any two eigenvectors, it can detect the similarity or closeness of the two eigenvectors as it approaches to 1. When $\left|\rho_{\boldsymbol{\Psi}_m\boldsymbol{\Psi}_n}\right|$ equals to unity, it indicates that $\boldsymbol{\Psi}_m$ and $\boldsymbol{\Psi}_n$ are perfectly correlated [48]; i.e. the two eigenvectors $\boldsymbol{\Psi}_m$ and $\boldsymbol{\Psi}_n$ coalesce to create at least a second order EPD. Hence, we first use it as a validation of a second order EPD. In Figure 12 (a), we plot all the possible magnitudes of the correlation coefficients between all the eigenvectors in $\underline{\mathbf{U}}$ (fifteen possibilities in our system). As expected, we observe the three EPDs illustrated in the dispersion diagram for real resonance frequencies (top plot in Figure 12 (a) to have a value

of the magnitude of the complex correlation coefficient $|\rho|$ equal to unity. Our ultimate goal is to validate the existence of a third order EPD as we did using the first figure of merit, hyper distance. Thus, we simply take the average of any two magnitudes of the complex correlation coefficients as

$$\bar{\rho} = \frac{1}{2}\left(\left|\rho_{\mathbf{\Psi}_m \mathbf{\Psi}_n}\right| + \left|\rho_{\mathbf{\Psi}_m \mathbf{\Psi}_l}\right|\right) \tag{3.7}$$

where $m = 1, 2, \ldots, 5$, $n = 2, 3, \ldots, 6$, $l = 3, 4, \ldots, 6$, and $m \neq n \neq l$ for our case. This average, $\bar{\rho}$, will be between 0 and 1 where 1 will indicate the occurrence of a third order EPD.

In Figure 12 (b) we plot all the possible averages of (3.7) (twenty possibilities in our case). Note that the average of two magnitudes of the complex correlation coefficients $\bar{\rho}$ here can only confirm the coalescence of three eigenvectors $\mathbf{\Psi}_m$, $\mathbf{\Psi}_n$, and $\mathbf{\Psi}_l$. Clearly, when

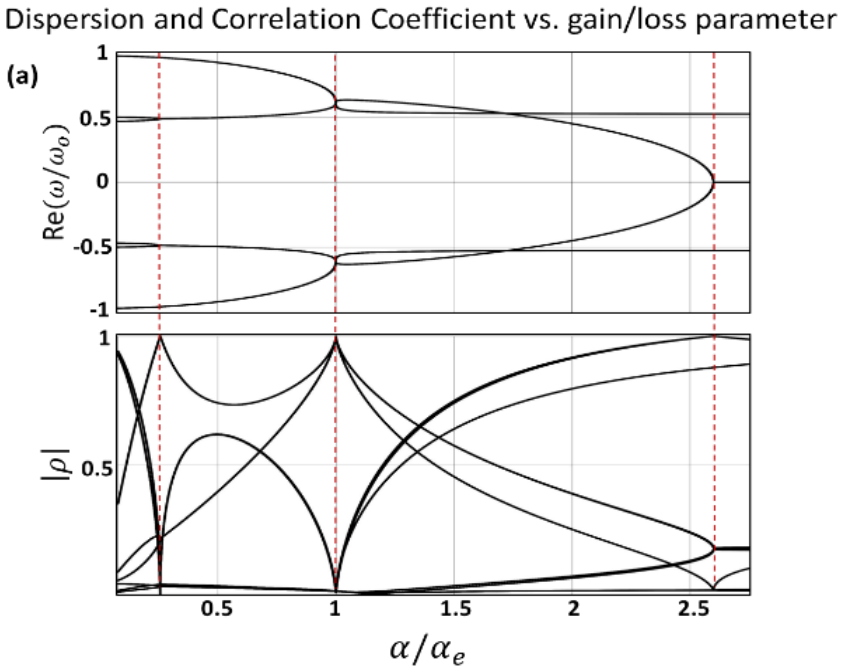

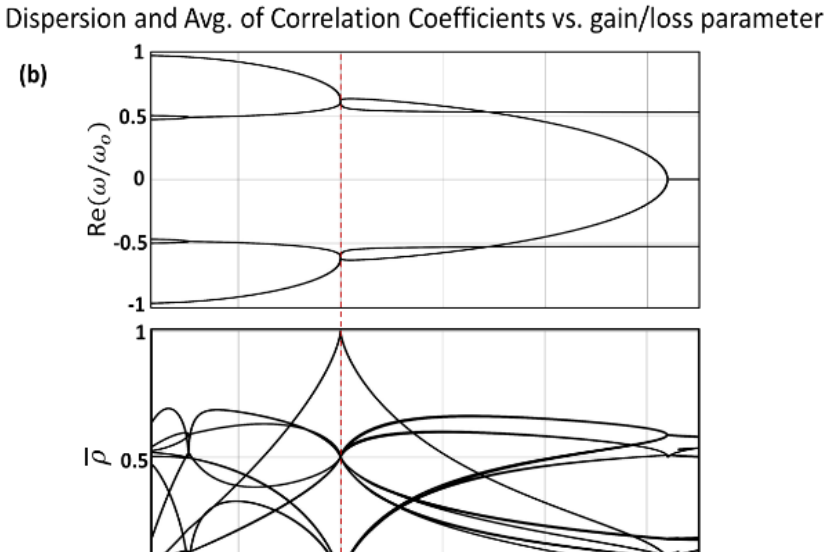

Figure 12: (a) Dispersion relation for real resonance frequency compared with the magnitude of the complex correlation coefficient. (b) Dispersion relation of the real frequency compared with the average of the magnitudes of the complex correlation coefficients. Validation of 3rd order EPD is shown in (b) as it only approaches 1 at the desired EPD.

$\alpha = \alpha_e$, the average of two magnitudes of the complex correlation coefficients becomes equal to unity which validates the occurrence of a third order EPD.

Sec. 3.2 Summary:

In this chapter we have validated the existence of a third order EPD point as well as second order EPD points. We used two techniques to confirm the coalescence of all the independent eigenvectors. The first one was the hyperdistance D_H technique where we showed it undergoes a minimum value only at third order EPD. The second method was the magnitude of complex correlation coefficient which on the other hand validated both second order EPD points and third order as its value approaches 1.

CHAPTER 4

TIME DOMAIN SOLUTION AND SIMULATION

In this chapter, we first analyze the coupled resonators (shown again here in Figure 13) time domain response by finding the explicit time domain functions of the state variables. Recall that we defined the state vector in Sec. 2.2 as $\mathbf{\Psi}(t)=\left[\begin{array}{cccccc} v_{C_1}(t) & v_{C_a}(t) & v_{C_2}(t) & i_{L_1}(t) & i_{L_a}(t) & i_{L_2}(t)\end{array}\right]^T$ where $v_{C_1}(t)$ for example is the voltage across the capacitor of the resonator associated with gain (i.e. the left side containing the negative resistor shown in Figure 13). The matrix equation representing the set of normal-from equations for our sixth order system was obtained in (2.5) and it is repeated here for convenience as

$$\frac{d\mathbf{\Psi}}{dt}=\underline{\mathbf{M}}\mathbf{\Psi}(t) \tag{4.1}$$

In the case of time-invariant coupled resonators components, the 6×6 system matrix $\underline{\mathbf{M}}$ contains constant elements (i.e. capacitors, inductors, and resistors), and $\frac{d\mathbf{\Psi}}{dt}$ and $\mathbf{\Psi}(t)$ are all vectors of six elements.

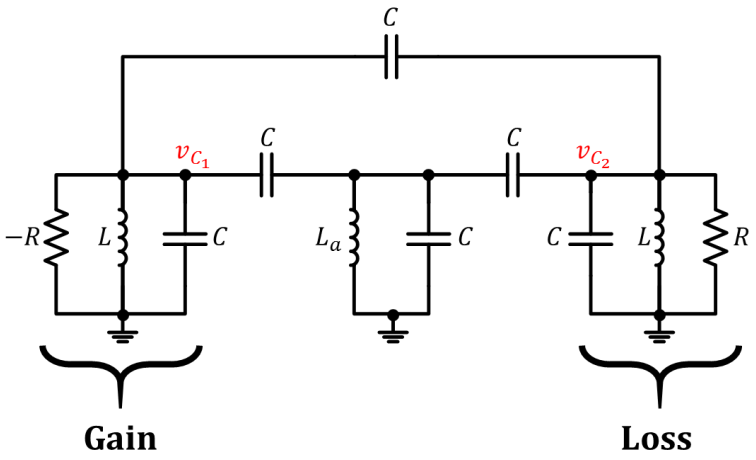

Figure 13: The third order EPD Coupled resonators showing the gain and loss sides.

For the full solution of the matrix equation, we must solve for $\boldsymbol{\Psi}(t)$, which is a linear combination of the six independent solutions $\boldsymbol{\Psi}_1(t), \boldsymbol{\Psi}_2(t), \ldots, \boldsymbol{\Psi}_6(t)$. Each must be found as a function of time which will provide every voltage and current in our coupled resonators. Ch.5 of [40] outlines the method for finding the matrix equation representing the set of equations general solution as follows:

- Obtain the eigenvalues of the system matrix by solving characteristic equation $\det(\underline{\mathbf{M}} - \lambda \underline{\mathbf{I}}) = 0$ where λ is the eigenvalue ($\lambda_1, \lambda_2, \ldots, \lambda_6$ for our case) and $\underline{\mathbf{I}}$ is the 6×6 identity matrix.
- Attempt to find the 6 linearly independent eigenvectors of matrix $\underline{\mathbf{M}}$ associated with the above eigenvalues. An eigenvector associated with the eigenvalue λ is a nonzero vector $\boldsymbol{\Psi}$ such that $\underline{\mathbf{M}}\boldsymbol{\Psi}=\lambda\boldsymbol{\Psi}$, which will lead to $(\underline{\mathbf{M}} - \lambda \underline{\mathbf{I}})\boldsymbol{\Psi} = 0$. Note $\boldsymbol{\Psi}$ represents the eigenvector of $\underline{\mathbf{M}}$.
- If the above step is possible, we obtain six linearly independent eigenvectors $\boldsymbol{\Psi}_1, \boldsymbol{\Psi}_2, \ldots, \boldsymbol{\Psi}_6$ and six linearly independent solutions

$$\boldsymbol{\Psi}_1(t) = \boldsymbol{\Psi}_1 e^{\lambda_1 t}, \quad \boldsymbol{\Psi}_2(t) = \boldsymbol{\Psi}_2 e^{\lambda_2 t}, \quad \ldots, \quad \boldsymbol{\Psi}_6(t) = \boldsymbol{\Psi}_6 e^{\lambda_6 t} \tag{4.2}$$

For this case the matrix equation representing the set of normal-from equations general solution is

$$\boldsymbol{\Psi}(t) = c_1 \boldsymbol{\Psi}_1(t) + c_2 \boldsymbol{\Psi}_2(t) + \ldots + c_6 \boldsymbol{\Psi}_6(t) \tag{4.3}$$

where $c_1, c_2, \ldots, c_6$ are constant coefficients that can be obtained from the initial conditions of the state variables.

Generally, the eigenvalues of any matrix can be distinct or repeated, real or complex. We will briefly investigate each of the cases of the different type of eigenvalues and find the corresponding general solution. It is necessary to recall that the eigenvalue $\lambda = j\omega$ is discussed in Sec. 2.2 where ω is the eigenfrequency of the coupled resonators. Thus, we can rewrite equation (4.2) as

$$\boldsymbol{\Psi}_1(t) = \boldsymbol{\Psi}_1 e^{j\omega_1 t}, \quad \boldsymbol{\Psi}_2(t) = \boldsymbol{\Psi}_2 e^{j\omega_2 t}, \quad \ldots, \quad \boldsymbol{\Psi}_6(t) = \boldsymbol{\Psi}_6 e^{j\omega_6 t} \tag{4.4}$$

Figure 14 is the dispersion diagram of the eigenfrequencies of the system as the gain/loss parameter increases which we obtained in Sec. 2.3 and Sec. 2.4. Here we highlight three regions as shown in Figure 14. The red colored region contains only real eigenfrequencies (distinct imaginary eigenvalues). The blue colored regions are where the complex eigenfrequencies located (distinct complex eigenvalues). Finally, the white colored regions show the EPD eigenfrequencies (repeated imaginary eigenvalues).

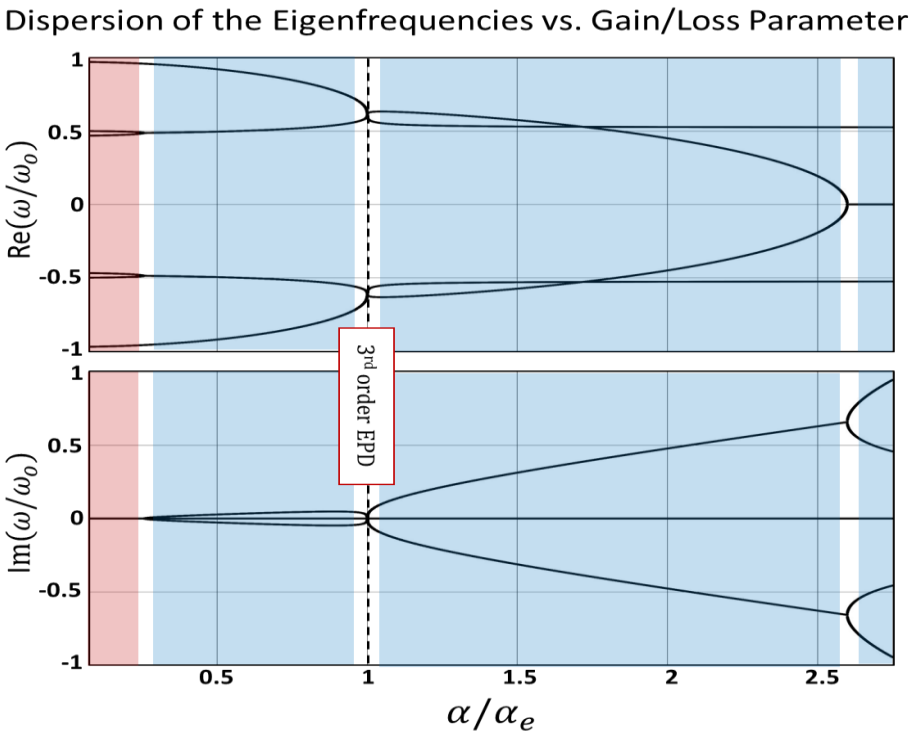

Figure 14: dispersion diagram of the eigenfrequencies highlighting three regions. Red: only real eigenfrequencies, blue: complex eigenfrequencies, and white: EPD eigenfrequencies. The dashed line is at the third order EPD.

Sec. 4.1 Distinct Real Eigenvalues (only imaginary eigenfrequency):

As shown in Figure 14, we do not obtain a case where only imaginary eigenfrequencies are presented. Therefore, our system matrix $\underline{\mathbf{M}}$ does not have a characteristic equation where its roots (the eigenvalues) are only distinct real eigenvalues. If this was not the case and we could get distinct real eigenvalues, the general solution will be as (4.3). This will cause an exponential growth or decay of the state variable These modes correspond to the overdamped modes of a single oscillator (Ch. 1 in [49]).

Sec. 4.2 Distinct complex conjugate Eigenvalues (complex eigenfrequency):

The method described previously is still valid if the eigenvalues are distinct. Therefore, the time evolution differential equation (4.1) will yield six linearly independent solutions, but the eigenvectors associated with the complex eigenvalues are also complex. This will lead to a complex general solution. Note that any complex eigenvalues must appear in complex conjugate pairs. We can obtain real valued solutions by taking the real and imaginary parts of a single complex-valued solution $\mathbf{\Psi}_1(t)$, one of the six independent solutions, associated with the complex eigenvalue λ. These two solutions (real and imaginary parts) will provide real-valued solutions corresponding to the two complex conjugate eigenvalues λ and λ^*. We consider one of the complex conjugate pair of the eigenvalues as $p+jq$ and its corresponding eigenvector is $\mathbf{\Psi}_1 = \mathbf{A}+j\mathbf{B}$ where $\mathbf{A}$ and $\mathbf{B}$ resemble real and imaginary N×1 vectors respectively (N = 6 in our case). The real and imaginary parts of the solutions $\mathbf{\Psi}_1(t)$ will appear respectively as

$$\begin{aligned} \mathrm{Re}\left[\mathbf{\Psi}_1(t)\right] &= e^{pt}\left(\mathbf{A}\cos qt - \mathbf{B}\sin qt\right) \\ \mathrm{Im}\left[\mathbf{\Psi}_1(t)\right] &= e^{pt}\left(\mathbf{B}\cos qt + \mathbf{A}\sin qt\right) \end{aligned} \tag{4.5}$$

which are associated with the complex conjugate eigenvalues $p \pm jq$.

These distinct complex eigenvalues are also complex eigenfrequencies which are displayed in the blue regions of Figure 14. To better understand the time domain response of the coupled resonators we use (4.5), but interchange p with q and change their signs since $\lambda = j\omega$. Depending on the signs of the complex eigenfrequencies, we can clearly expect

the mode time domain response. The mode will exponentially grow and decay due to the imaginary eigenfrequencies, both of which oscillate at frequencies caused by the real eigenfrequencies shown in Figure 14. We illustrate this case by simulating the time domain evolution of the capacitance voltage in the resonator with gain $v_{C_1}(t)$. The transient behavior of the coupled resonators is simulated using the time domain solver Keysight ADS. In Figure 15 we show the time domain simulation of the absolute value of the state variable $v_{C_1}(t)$ with an initial condition $v_{C_1}(0^-) = 0.01\,\text{V}$ on the capacitor C in the resonator with gain . The gain/loss parameter α, is chosen here to be slightly less than α_e (in the blue region of Figure 14) $\alpha = 0.85\alpha_e$. The other parameters of the coupled resonators are set as $C = 330\,\text{pF}$, $L = 10\,\mu\text{H}$, $L_a \approx 12\,\mu\text{H}$, and $\alpha_e = 10.9\times10^4\,\frac{\text{S}}{\text{F}}$ (or per second). In this example, we plot the absolute value of the $v_{C_1}(t)$ showing only the exponentially growth in addition to an oscillatory behavior (red line) and the average of the absolute value of the $v_{C_1}(t)$ (black line). The results of Figure 15 agree with our expectations mentioned above.

In the case of only distinct imaginary eigenvalues i.e. pure real eigenfrequencies as presented in the red region of Figure 14, there are six purely real eigenfrequencies that come in three sets of positive-negative pairs. The behavior in this regime is simply oscillatory and occurs at three distinct eigenfrequencies since the positive and negative frequencies of equal magnitude are essentially identical.

We can prove the oscillatory behavior mentioned above by using (4.4) and substituting each ω by the purely real eigenfrequencies ω_r so that the solutions will be proportional to

$e^{\pm j\omega_r t}$. In Figure 16, We illustrate this behavior by simulating the time domain evolution of the magnitude capacitance voltage in the resonator with gain of the coupled resonator (left side) (i.e. $v_{C_1}(t)$) with the same initial condition and parameters

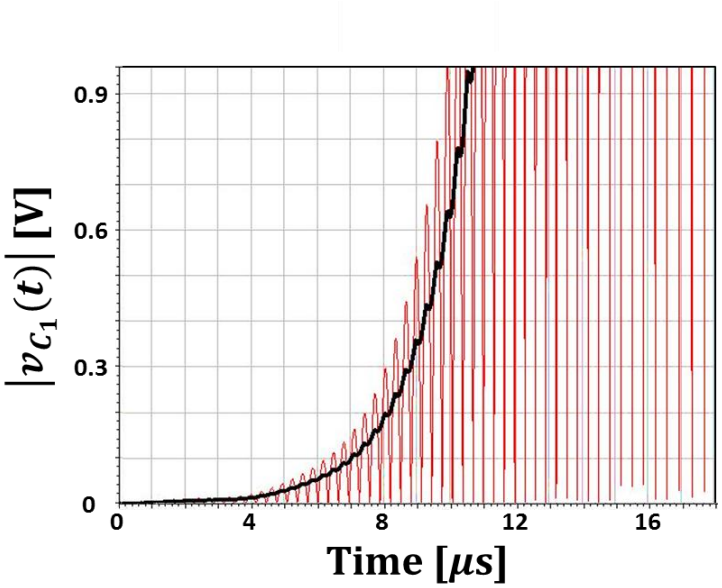

Figure 15: The simulated absolute value of the time domain voltage across the capacitor in the resonator with gain in the presence of complex eigenfrequencies. Red colored lines represent the actual absolute voltage and the black colored line is its average. The mode is exponentially growing with oscillations.

values used in the previous case except the gain/loss parameter here is $\alpha = 0.1\alpha_e$ (in the red region of Figure 14).

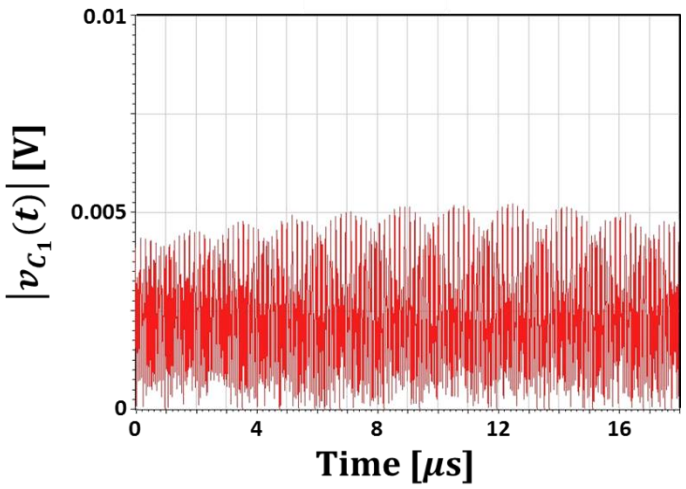

Figure 16: The time domain results of the magnitude of the capacitor voltage at the resonator with gain is simulated where the eigenfrequencies are purely real. The behavior of this mode is simply oscillatory. The mode here is just oscillatory.

Sec. 4.3 Repeated Eigenvalues (Repeated eigenfrequency):

In this section we discuss the general solution of the matrix equation when the characteristic equation of the system, $\det\left(\underline{\mathbf{M}} - \lambda \underline{\mathbf{I}}\right) = 0$, does not have only distinct roots but has at least one repeated root. In general, an eigenvalue is of multiplicity (or algebraic multiplicity) p if it is a p-fold root of the characteristic equation. For an eigenvalue of multiplicity $p > 1$, there might be fewer than p linearly independent associated eigenvectors. As a result, we cannot find a complete set of six linearly independent eigenvectors of $\underline{\mathbf{M}}$. But an eigenvalue of multiplicity p will be called complete if it has p linearly independent associated eigenvectors. In this case a general solution of the time evolution differential equation (4.1) is still given by (4.4). However, the eigenvalues of $\underline{\mathbf{M}}$ for the EPD case are not complete, they are called defective instead since the number of

linearly independent eigenvectors is less than the multiplicity p as discussed in Sec. 2.3.

Ch.5 of [40] defines an eigenvalue λ of multiplicity p defective if it has $l < p$ linearly independent eigenvectors. The defect number $d = p - l$ provides the number of missing eigenvectors of the defective eigenvalue. Thus, our third order EPD has multiplicity $p = 3$ and defect $d = 2$. To find the linearly independent solutions of $\frac{d\boldsymbol{\Psi}}{dt} = \underline{\mathbf{M}}\boldsymbol{\Psi}(t)$, we need to find the generalized eigenvectors. The third order EPD has multiplicity 3 of eigenvalue λ_e which requires 3 generalized eigenvectors $\{\boldsymbol{\Psi}_1, \boldsymbol{\Psi}_2, \boldsymbol{\Psi}_3\}$. The third order EPD generalized eigenvector $\boldsymbol{\Psi}_3$ associated with the eigenvalue λ_e of multiplicity $p = 3$ of the matrix $\underline{\mathbf{M}}$ is obtained by

$$\left(\underline{\mathbf{M}} - \lambda_e \underline{\mathbf{I}}\right)^3 \boldsymbol{\Psi}_3 = 0 \quad \text{and} \quad \left(\underline{\mathbf{M}} - \lambda_e \underline{\mathbf{I}}\right)^2 \boldsymbol{\Psi}_3 \neq 0 \tag{4.6}$$

such that the eigenvectors

$$\boldsymbol{\Psi}_2 = \left(\underline{\mathbf{M}} - \lambda_e \underline{\mathbf{I}}\right)\boldsymbol{\Psi}_3 \quad \text{and} \quad \boldsymbol{\Psi}_1 = \left(\underline{\mathbf{M}} - \lambda_e \underline{\mathbf{I}}\right)\boldsymbol{\Psi}_2 \tag{4.7}$$

are both nonzero. Then the three linearly independent solutions of the rate matrix equation $\frac{d\boldsymbol{\Psi}}{dt} = \underline{\mathbf{M}}\boldsymbol{\Psi}(t)$ are equal to

$$\begin{aligned} \boldsymbol{\Psi}_1(t) &= \boldsymbol{\Psi}_1 e^{\lambda_e t} \\ \boldsymbol{\Psi}_2(t) &= \left(\boldsymbol{\Psi}_1 t + \boldsymbol{\Psi}_2\right) e^{\lambda_e t} \\ \boldsymbol{\Psi}_3(t) &= \left(\frac{1}{2}\boldsymbol{\Psi}_1 t^2 + \boldsymbol{\Psi}_2 t + \boldsymbol{\Psi}_3\right) e^{\lambda_e t} \end{aligned} \tag{4.8}$$

Since $\lambda_e = j\omega_e$ and ω_e is purely real at $\alpha = \alpha_e$ (the middle white region of Figure 14), we observe that when using (4.8) the real eigenfrequencies only cause the general solution to be a oscillatory in time. Thus, we expect the mode to have a quadratic increase and decrease. The quadratic growth is unique to having a third order EPD as we showed in (4.8) . To illustrate this, we simulate the time domain evolution of the magnitude of capacitance voltage $v_{C_1}(t)$ shown in Figure 17. The initial condition and all of the parameters are similar to the previous cases except the loss/gain parameter now is $\alpha = \alpha_e$.

Evidently, we observe here the dominant quadratic growth in the voltage across the capacitor of the resonator with gain since the system has a third order EPD.

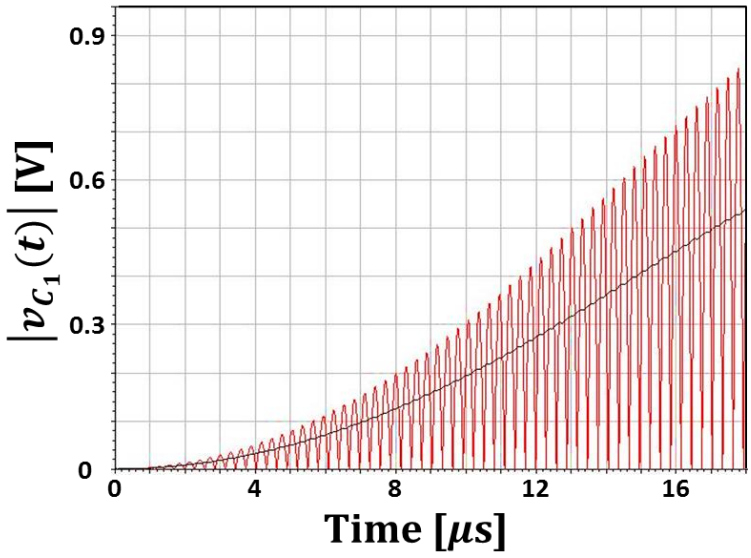

Figure 17: The simulated absolute value of the time domain of the voltage across the capacitor in the resonator with gain at the third order EPD. Red colored lines represent the actual absolute voltage of $v_{C_1}(t)$ and the black colored line is its average. Although we have only a pure real frequency, we observe the quadratic growth in this plot due to the 3rd order EPD.

From (4.8), we clearly expect a dominant quadratically growing modes as an

an indication of the occurrence of the third order EPD since this equation is valid only if generalized eigenvectors are needed which is the case for EPD. To validate our conclusion that Figure 17 exhibits a quadratic growth, we compare the average of the absolute capacitance voltage $v_{C_1}(t)$ (black colored line in Figure 17) with three different curves using the curve fitting tool in MATLAB (shown in Figure 18).

The first fitted curve shown in Figure 18 (a) is linear growth which would be an indication of a second order EPD as in [26]. While the second fitted curve in Figure 18 (b) is an exponential growth (similar to the behavior we observed in Figure 15). Finally, we curve

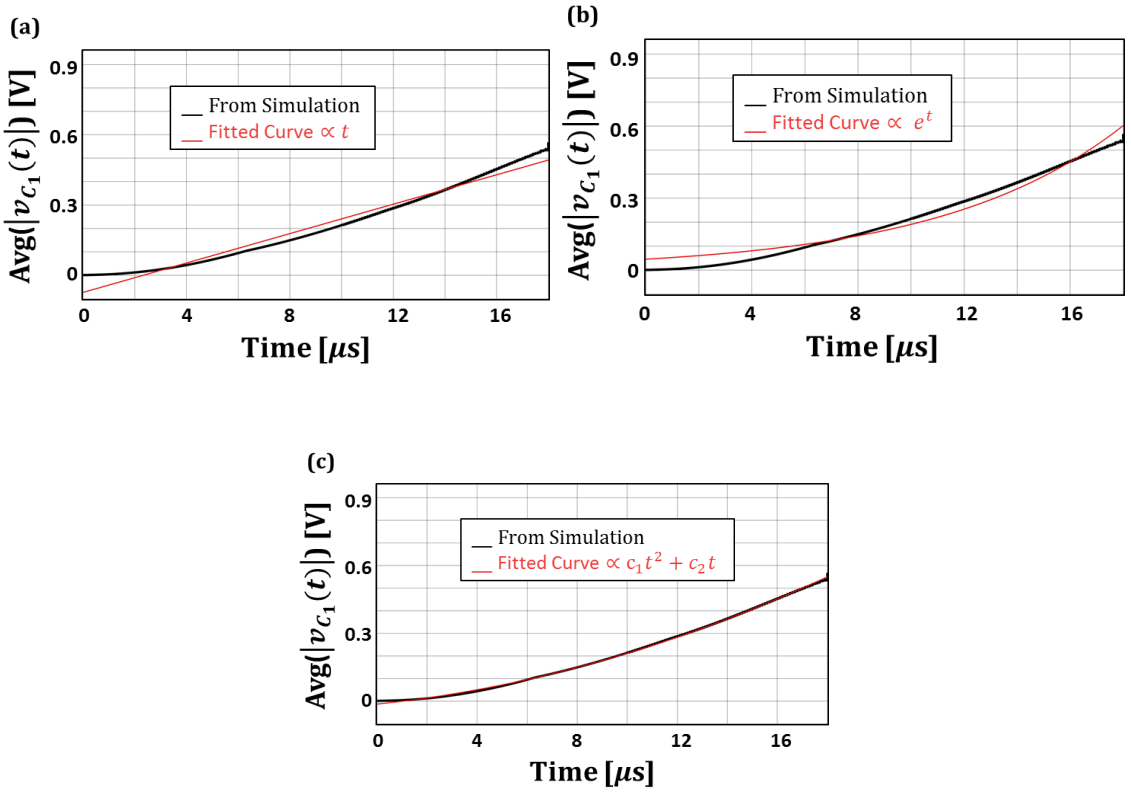

Figure 18: Average of the simulated absolute capacitance voltage of the resonator with gain results at the 3rd order EPD curve fitted. (a) Comparison of simulation with fitted linear growth (b) with fitted exponential growth and (c) with fitted quadratic growth where c_1 and c_2 are just constants. Clearly figure (c) shows perfect agreement between the fitted curve and the curve from simulation, indicating the quadratic algebraic growth.

fit the simulation results with a quadratic growth shown in Figure 18 (c). Evidently, we observe the best fitted curve is in Figure 18 (c) where we fit a quadratic function to our simulation results. Remarkably, at the third order EPDs the eigenstates of the coupled resonators grow quadratically even when the resonance frequency is purely real.

Sec. 4.4 Summary:

In this chapter we examined the coupled resonators in the time domain. We showed the exponential growth with oscillation condition of the coupled resonators, i.e., when the system has complex conjugate eigenfrequencies and in purely real resonance frequencies where the eigenstate only oscillate. Finally, at the third order EPDs the eigenstates of the coupled resonators grow quadratically even when the resonance frequency is purely real. Moreover, we have illustrated how such temporally induced EPDs may have potential applications in the development of very accurate sensing devices by demonstrating how sensitive the third order coupled resonators to small perturbations. The time domain solver ADS simulations of the three conditions of the coupled resonators they undergo by changing the loss/gain parameter were also shown. We finally validated the quadratic growth of the eigenstate of the coupled resonators at the third order EPD using the curve fitting tool in MATLAB in which we showed a confirmation of our expectations.

CHAPTER 5

CONCLUSION AND FUTURE WORK

We have demonstrated in this thesis that the coupled resonators which consist of an LC tank coupled with two RLC oscillators one with amplification and the other with equivalent attenuation, exhibit a third order EPD. We have also discussed the necessary conditions to realize a third order EPD in the coupled resonators. Using the necessary conditions, we showed the dispersion of the eigenfrequencies of the system versus the loss/gain parameter by using the state variable method. We then compared the state variable method with the transverse resonance method which does not require information about the state variables and only rely on the system parameters. Furthermore, we have proven the existence of EPDs in the coupled resonators by using the hyperdistance and magnitude of the complex correlation coefficient methods. Analysis in the time domain of the coupled resonators was shown in the exponential growth with oscillation condition, i.e., when the system has complex conjugate eigenfrequencies and in purely real resonance frequencies where the eigenstate only oscillate. Finally, at the third order EPDs the eigenstates of the coupled resonators grow quadratically even when the resonance frequency is purely real. Moreover, we have illustrated how such temporally induced EPDs may have potential applications in the development of very accurate sensing devices by demonstrating how sensitive the third order coupled resonators to small perturbations. The time domain solver ADS simulations of the three conditions of the coupled resonators they undergo by changing the loss/gain parameter are also shown.

Further practical analysis of the third coupled resonators are currently in final optimization process, as of June of 2018. We are constructing the coupled resonators to operate at radio frequencies. It is important to note that the physical resonators differ substantially from the ideal resonators as the attempt to balance the configuration is limited by the components tolerances and thermal and temporal drifts. Therefore, we acquired components with very low tolerances and that are also tunable to obtain the desired third order EPD. We will then implement these coupled resonators to operate as sensors that are very accurate.

REFERENCES

[1] J. Wiersig, "Enhancing the Sensitivity of Frequency and Energy Splitting Detection by Using Exceptional Points: Application to Microcavity Sensors for Single-Particle Detection," *Phys. Rev. Lett.*, vol. 112, no. 20, p. 203901, May 2014.

[2] W. Chen, Ş. K. Özdemir, G. Zhao, J. Wiersig, and L. Yang, "Exceptional points enhance sensing in an optical microcavity," *Nature*, vol. 548, no. 7666, pp. 192–196, Aug. 2017.

[3] W. D. Heiss, "The physics of exceptional points," *J. Phys. A: Math. Theor.*, vol. 45, no. 44, p. 444016, 2012.

[4] C. Dembowski *et al.*, "Experimental observation of the topological structure of exceptional points," *Phys. Rev. Lett.*, vol. 86, no. 5, pp. 787–790, Jan. 2001.

[5] T. Stehmann, W. D. Heiss, and F. G. Scholtz, "Observation of exceptional points in electronic circuits," *Journal of Physics A: Mathematical and General*, vol. 37, no. 31, pp. 7813–7819, Aug. 2004.

[6] M. Liertzer, L. Ge, A. Cerjan, A. D. Stone, H. E. Türeci, and S. Rotter, "Pump-Induced Exceptional Points in Lasers," *Phys. Rev. Lett.*, vol. 108, no. 17, p. 173901, Apr. 2012.

[7] B. Zhen *et al.*, "Spawning rings of exceptional points out of Dirac cones," *Nature*, vol. 525, no. 7569, pp. 354–358, Sep. 2015.

[8] F. Vollmer and L. Yang, "Review Label-free detection with high-Q microcavities: a review of biosensing mechanisms for integrated devices," *Nanophotonics*, vol. 1, no. 3–4, pp. 267–291, 2012.

[9] L. He, Ş. K. Özdemir, J. Zhu, W. Kim, and L. Yang, "Detecting single viruses and nanoparticles using whispering gallery microlasers," *Nature Nanotechnology*, vol. 6, no. 7, pp. 428–432, Jul. 2011.

[10] Y. Liu, J. A. R. Williams, and I. Bennion, "Optical bend sensor based on measurement of resonance mode splitting of long-period fiber grating," *IEEE Photonics Technology Letters*, vol. 12, no. 5, pp. 531–533, May 2000.

[11] C. E. Rüter, K. G. Makris, R. El-Ganainy, D. N. Christodoulides, M. Segev, and D. Kip, "Observation of parity–time symmetry in optics," *Nature Physics*, vol. 6, no. 3, pp. 192–195, Mar. 2010.

[12] H. Ramezani, T. Kottos, R. El-Ganainy, and D. N. Christodoulides, "Unidirectional nonlinear $\mathcal{PT}$-symmetric optical structures," *Phys. Rev. A*, vol. 82, no. 4, p. 043803, Oct. 2010.

[13] J. Schindler, A. Li, M. C. Zheng, F. M. Ellis, and T. Kottos, "Experimental study of active LRC circuits with PT-symmetries," *Phys. Rev. A*, vol. 84, no. 4, p. 040101, Oct. 2011.

[14] M. Kulishov and B. Kress, "Distributed Bragg reflector structures based on PT-symmetric coupling with lowest possible lasing threshold," *Opt Express*, vol. 21, no. 19, pp. 22327–22337, Sep. 2013.

[15] H. Hodaei, M.-A. Miri, M. Heinrich, D. N. Christodoulides, and M. Khajavikhan, "Parity-time–symmetric microring lasers," *Science*, vol. 346, no. 6212, pp. 975–978, Nov. 2014.

[16] H. Hodaei *et al.*, "Enhanced sensitivity at higher-order exceptional points," *Nature*, vol. 548, no. 7666, pp. 187–191, Aug. 2017.
[17] M. A. K. Othman, V. Galdi, and F. Capolino, "Exceptional points of degeneracy and PT-symmetry in photonic coupled chains of scatterers," *Physical Review B*, vol. 95, no. 10, Mar. 2017.
[18] M. Veysi, M. A. K. Othman, A. Figotin, and F. Capolino, "The degenerate band edge laser: a new paradigm for coherent light-matter interaction," *Physical Review B*, vol. 97, no. 19, May 2018.
[19] C. M. Bender and S. Boettcher, "Real Spectra in Non-Hermitian Hamiltonians Having PT Symmetry," *Physical Review Letters*, vol. 80, no. 24, pp. 5243–5246, Jun. 1998.
[20] A. Guo *et al.*, "Observation of PT-Symmetry Breaking in Complex Optical Potentials," *Phys. Rev. Lett.*, vol. 103, no. 9, p. 093902, Aug. 2009.
[21] J. Gear, F. Liu, S. T. Chu, S. Rotter, and J. Li, "Parity-time symmetry from stacking purely dielectric and magnetic slabs," *Physical Review A*, vol. 91, no. 3, Mar. 2015.
[22] R. El-Ganainy, K. G. Makris, D. N. Christodoulides, and Z. H. Musslimani, "Theory of coupled optical PT-symmetric structures," *Opt. Lett., OL*, vol. 32, no. 17, pp. 2632–2634, Sep. 2007.
[23] I. V. Barashenkov, L. Baker, and N. V. Alexeeva, "PT-symmetry breaking in a necklace of coupled optical waveguides," *Physical Review A*, vol. 87, no. 3, Mar. 2013.
[24] Z. H. Musslimani, K. G. Makris, R. El-Ganainy, and D. N. Christodoulides, "Optical Solitons in PT Periodic Potentials," *Phys. Rev. Lett.*, vol. 100, no. 3, p. 030402, Jan. 2008.
[25] M. Kang, F. Liu, and J. Li, "Effective spontaneous PT-symmetry breaking in hybridized metamaterials," *Phys. Rev. A*, vol. 87, no. 5, p. 053824, May 2013.
[26] H. Kazemi, M. Y. Nada, T. Mealy, A. F. Abdelshafy, and F. Capolino, "Exceptional points of degeneracy induced by linear time-periodic variation," *arXiv:1804.01075 [physics]*, Apr. 2018.
[27] A. Figotin and I. Vitebskiy, "Gigantic transmission band-edge resonance in periodic stacks of anisotropic layers," *Phys. Rev. E*, vol. 72, no. 3, p. 036619, Sep. 2005.
[28] C. D. Meyer, Ed., *Matrix Analysis and Applied Linear Algebra*. Philadelphia, PA, USA: Society for Industrial and Applied Mathematics, 2000.
[29] L. Hogben, Ed., *Handbook of Linear Algebra, Second Edition*, 2 edition. Boca Raton, Florida: Chapman and Hall/CRC, 2013.
[30] A. Figotin and I. Vitebskiy, "Oblique frozen modes in periodic layered media," *Phys Rev E Stat Nonlin Soft Matter Phys*, vol. 68, no. 3 Pt 2, p. 036609, Sep. 2003.
[31] S. L. McCall, A. F. J. Levi, R. E. Slusher, S. J. Pearton, and R. A. Logan, "Whispering-gallery mode microdisk lasers," *Appl. Phys. Lett.*, vol. 60, no. 3, pp. 289–291, Jan. 1992.
[32] M. A. K. Othman, M. Veysi, A. Figotin, and F. Capolino, "Low Starting Electron Beam Current in Degenerate Band Edge Oscillators," *IEEE Transactions on Plasma Science*, vol. 44, no. 6, pp. 918–929, Jun. 2016.
[33] D. Oshmarin *et al.*, "Oscillator Based on Lumped Double Ladder Circuit with Band Edge Degeneracy," *arXiv:1610.00415 [physics]*, Oct. 2016.
[34] M. A. K. Othman, M. Veysi, A. Figotin, and F. Capolino, "Giant amplification in degenerate band edge slow-wave structures interacting with an electron beam," *Physics of Plasmas*, vol. 23, no. 3, p. 033112, Mar. 2016.
[35] M. A. K. Othman, V. A. Tamma, and F. Capolino, "Theory and New Amplification Regime in Periodic Multimodal Slow Wave Structures With Degeneracy Interacting With an

Electron Beam," *IEEE Transactions on Plasma Science*, vol. 44, no. 4, pp. 594–611, Apr. 2016.
[36] C. Peng, Z. Li, and A. Xu, "Rotation sensing based on a slow-light resonating structure with high group dispersion," *Appl. Opt., AO*, vol. 46, no. 19, pp. 4125–4131, Jul. 2007.
[37] M. A. K. Othman and F. Capolino, "Coupled transmission line array antennas with exceptional points of degeneracy," in *2017 IEEE International Symposium on Antennas and Propagation USNC/URSI National Radio Science Meeting*, 2017, pp. 57–58.
[38] Mohazzab, J. Hussain, Q. Mohsin, and Sattar, "RLC Circuit Response and Analysis (Using State Space Method)," May 2018.
[39] W. H. Hayt, J. E. Kemmerly, and S. Durbin, *Engineering Circuit Analysis*, 6th edition. New York: McGraw Hill Higher Education, 2002.
[40] C. H. Edwards and D. E. Penney, *Elementary Differential Equations with Boundary Value Problems*, 6 edition. Upper Saddle River, NJ: Pearson, 2007.
[41] M. Y. Nada, M. A. K. Othman, and F. Capolino, "Theory of Coupled Resonator Optical Waveguides (CROW) Exhibiting High Order Exceptional Points of Degeneracy," *Physical Review B*, vol. 96, no. 18, Nov. 2017.
[42] T. Itoh, Ed., *Numerical Techniques for Microwave and Millimeter-Wave Passive Structures*, 1 edition. New York: Wiley-Interscience, 1989.
[43] K. Chang, *Encyclopedia of RF and Microwave Engineering, 6 Volume Set*. Wiley, 2005.
[44] M. Othman, "Dispersion engineering of photonic and high-power devices with exceptional points of degeneracy," UC Irvine, 2017.
[45] J. L. Rodgers and W. A. Nicewander, "Thirteen Ways to Look at the Correlation Coefficient," *The American Statistician*, vol. 42, no. 1, pp. 59–66, 1988.
[46] D. H. Johnson and D. E. Dudgeon, *Array Signal Processing: Concepts and Techniques*. New York, NY, USA: Simon & Schuster, Inc., 1992.
[47] F. Weissgerber, E. Colin-Koeniguer, N. Trouve, and J. M. Nicolas, "Statistics for complex correlation coefficients applied to advanced SAR modes: Interferometry and polarimetry," in *2014 International Radar Conference*, 2014, pp. 1–6.
[48] H. Khenouchi, Y. Smara, M. Migliaccio, F. Nunziata, and A. Buono, "The Modulus of the Complex Correlation Coefficient Between Co-Polarized Channels for Oil Spill Observation," presented at the Living Planet Symposium, 2016, vol. 740, p. 219.
[49] J. Schindler, "PT-Symmetric Electronics," *Masters Theses*, May 2013.